# Range-Energy Relations for Electrons and the Determination of Beta-Ray End-Point Energies by Absorption

L. KATZ AND A. S. PENFOLD*

*University of Saskatchewan, Saskatoon, Saskatchewan, Canada*

It is shown that for aluminum absorbers, a single range-energy equation $R=412\,E_0^{1.265-0.0954\ln E_0}$ (mg/cm²) will fit the most reliable published values of practical ranges of monoenergetic electrons and the maximum ranges of nuclear beta-rays in the energy region $0.01\leqslant E_0\leqslant 2.5$ Mev. The average deviation of 59 monoenergetic measurements from this equation is +0.08 percent in energy, and −0.05 percent in energy for 35 beta-ray measurements. The mean deviation is 4.1 percent in each case. There are few ranges for energies above 2.5 Mev. All the higher energy values found in the literature and four new measurements on monoenergetic electrons are presented and are shown to be consistent with the range-energy equation $R=530\,E_0-106$ (mg/cm²) for $E_0\geqslant 2.5$ Mev. It is shown that the curve $(dE_0/dR)$ is nearly parallel to the theoretical curve for the rate of energy loss by ionization in the region between 0.01 and 20 Mev and is about 25 percent larger. The reason for this discrepancy is not known. All the methods commonly used to determine the ranges of beta-rays from absorption curves are discussed and a new method developed by the authors is presented.

## INTRODUCTION

THE absorption method is still widely used for determining electron energies of both monoenergetic and nuclear beta-rays from their range in aluminum, though in most cases with some hesitation. This hesitation probably stems from the fact that a careful examination of the method, its advantages and limitations, has not been available to data.

The successful application of the absorption method also depends on one's ability to translate range measurements into electron energy. For this purpose an accurate graph or empirical equation between range and energy is required. Quite apart from electron energy measurements, the range-energy curve is of some theoretical interest because of its bearing on the rate of energy loss by electrons through ionization.

In particular, one of the problems in beta-ray spectroscopy is the accurate determination of the end-point energy (maximum energy) of the beta-rays emitted by radioactive nuclei. A knowledge of the beta- and gamma-ray energies along with the decay scheme allows one to evaluate the mass difference between the parent and daughter nuclei[1] as well as the energy levels of the daughter nucleus. In the case of positron decay the rate of $K$-capture to $\beta^+$-emission is strongly dependent on the end-point energy, and a knowledge of it allows the observed ratio to be checked with that predicted by theory.

Actually there are at present only two methods by which the end-point energy (maximum energy) of a beta-ray spectrum may be determined: either with the use of a beta-ray spectrometer or by absorption of the rays in some material.

When a beta-ray spectrometer is used, the beta-rays are resolved with a magnetic field and the number emitted in each momentum (or energy) interval is determined. The end-point energy might then be determined by inspection of the number-momentum curve. However, this procedure has been found to be inaccurate in many cases and so a Kurie plot[2,3] is made. The method of the Kurie plot was first proposed for use with allowed transitions, as defined by the Fermi theory of beta-decay.[4,5] If the data so plotted do not form a straight line (or a series of straight lines), then the transition is assumed to be forbidden and an attempt is made to find a correction factor (a factor which varies with the degree of forbiddeness) which will make the experimental points form a straight line when plotted in a modified Kurie plot.

If the transition is allowed, the method is straightforward, and, provided that sources of sufficient intensity are available, accurate end-point energies and branching ratios, in the case of complex spectra, may be obtained. In the case of forbidden transitions, considerable difficulty may be experienced in determining the proper correction factor.

The success of the second method, that of absorption, depends on a knowledge of a relation between the end-point energy of the beta-rays and their range in some standard material, usually aluminum.[6,7]

If the fractions of the incident betas which pass through given thicknesses of aluminum are plotted against those thicknesses an absorption curve is ob-

* Now at the University of Illinois, Department of Physics, Champaign, Illinois.

[1] A. G. G. Mitchell, Revs. Modern Phys. **22**, 36 (1950).

[2] Kurie, Richardson, and Paxton, Phys. Rev. **49**, 368 (1936).

[3] F. N. P. Kurie, Phys. Rev. **73**, 1207 (1948).

[4] Enrico Fermi, Z. Physik **88**, 161 (1934).

[5] E. J. Konopinski and G. E. Uhlenbeck, Phys. Rev. **60**, 308 (1941).

[6] N. Feather, Phys. Rev. **35**, 1559 (1930).

[7] L. E. Glendenin, Nucleonics **2**, 12 (1948).

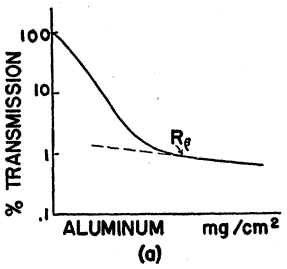


FIG. 1(a). Percent of nuclear beta-rays transmitted by various thickness of aluminum absorber. The background is the result of cosmic rays, natural radioactivity, and Compton electrons from $\gamma$-rays, when present. The point at which the absorption curve meets the background is called the range ($R_\beta$) of the betas.

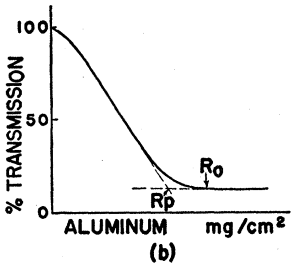


FIG. 1(b). Characteristic absorption curve of homogeneous electrons in aluminum. Point where extension of the linear portion of the curve meets the background is called the practical range, $R_p$. The maximum range $R_0$ is the point where the absorption curve runs into the background.

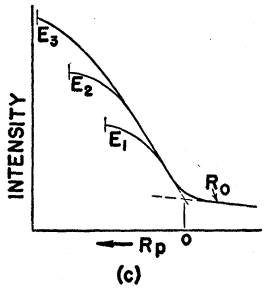


FIG. 1(c) Sketch to show how absorption curves of homogeneous electrons of different initial energy have the same shape near the end of their range. Curves of initial energy $E_1$, $E_2$, and $E_3$ are drawn with their practical ranges, $R_p$, coincident.

tained (Fig. 1(a)). At high filter thicknesses the curve passes into the background. This background is usually due to cosmic rays, and gamma-rays when they are present. The point at which the absorption curve meets the background is called the range. The existence of such a range was first pointed out by Gray in 1912.[8] Once the range has been measured, the end-point energy can be determined from the range-energy relation.

To date, the absorption method has not yielded results comparable in accuracy to the best magnetic spectrometer method. While the absorption method has the advantages of simplicity, speed, and, above all, sensitivity, it does not present a "picture" of the spectrum. Conversion peaks (particularily if they occur near the end-point) and Compton recoil electrons are hidden factors which may lead to a value for the range that is in considerable error.

Usually, however, results of fair accuracy (2–10 percent) may be obtained with comparatively weak sources. For example, the highest specific activity of $Cu^{62}$ (10.1 minute half-life), obtainable from the irradiation of copper by the University of Saskatchewan betatron was about $10^6$ counts per minute per gram. The activity was more than enough to permit an excellent absorption curve to be determined, but this would be a weak source for a spectrometer.

Notwithstanding the criticisms of the absorption method, the authors felt that because of its great sensitivity the method merited further study.

Any discussion of the absorption method should consider both the method of determining the range and the range-energy relation required to convert the range into an end-point energy.

In this paper, the authors discuss the previously used methods of determining ranges as well as an original method which has been used by them with considerable success.[9,10] A comprehensive summary of experimentally determined range-energy points is presented, and it is found that a single empirical relation will describe the results in the region 0.01 Mev to 2.5 Mev (0.1 to 1200 mg/cm²).

## RANGE-ENERGY RELATIONS

Early range-energy measurements were made mainly with nearly homogeneous (monoenergetic) beams of electrons. The absorption curves for these have a long straight portion down to fairly low intensities (intensity plotted to a linear scale) and then a considerable tail, going into the background (Fig. 1(b)). After the electrons have penetrated a certain fraction of their range the beam becomes completely diffuse and so all absorption curves have the same shape near the range thickness as is shown in Fig. 1(c). Because of this similarity in shape some writers[11,12] have defined the point at which the extension of the linear region meets the background as the *practical range* ($R_p$), whereas the point were the tail meets the background is known as the *maximum range* ($R_0$).[13] Thus, for homogeneous electrons one has, in $R_p$, a consistent definition of the range.

However, no linear region exists for beta-ray absorption curves, and the definition of the range is more arbitrary. Since range determination by inspection is usually inaccurate, a method of absorption curve analysis is used. There are a number of such methods in current use. If such a method is used, then that method constitutes a definition of the range for beta-rays, usually designated by $R_\beta$.

If the various methods of absorption curve analysis

[8] J. A. Gray, Proc. Roy. Soc. (London) **87A**, 487 (1912); also Trans. Roy. Soc. Can. **16**, III, 125 (1922).

[9] Katz, Penfold, Moody, Haslam, and Johns, Phys. Rev. **77**, 289 (1950).

[10] Haslam, Katz, Moody, and Skarsgard, Phys. Rev. **80**, 318 (1950).

[11] E. Bleuler and W. Zunti, Helv. Phys. Acta **19**, 375 (1946).

[12] F. L. Hereford and C. P. Swann, Phys. Rev. **78**, 727 (1950).

[13] E. Bleuler and W. Zunti have called these the *practical maximum range and absolute maximum range.*

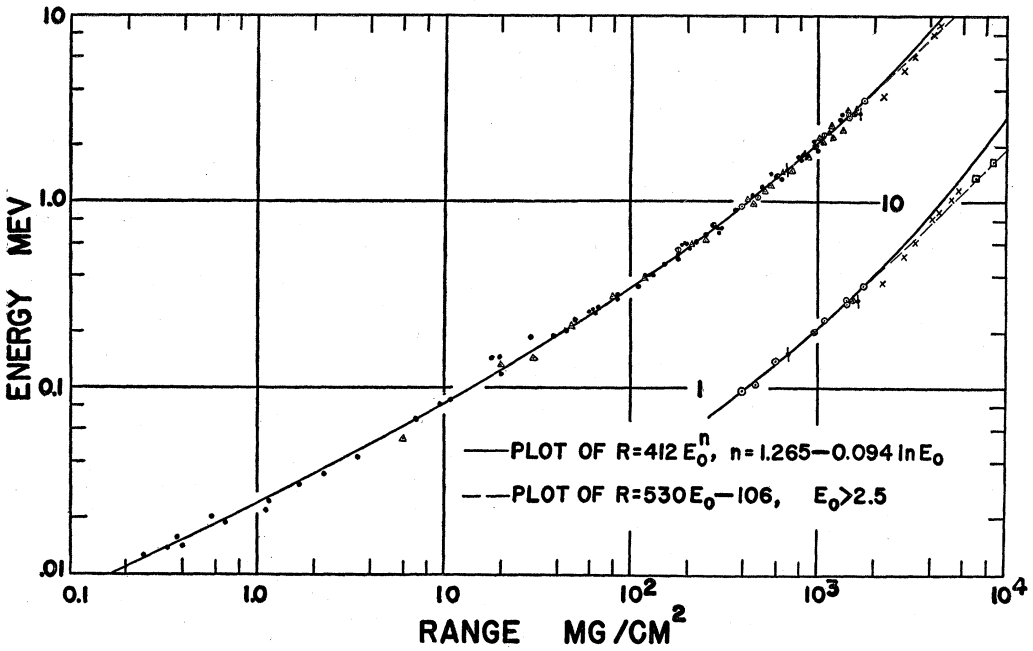


FIG. 2. Range-energy curve. The experimental points are those listed in Table I. ● Practical range of homogeneous electrons as measured by Varder, Schonland, Madgwick, Eddy, Marshall and Ward. ⊗ Practical range of homogeneous electrons according to Trump, Wright, and Clarke. △ Ranges of beta-rays according to measurements of Widdowson and Champion, Moore, and Glendenin; energies are the best accepted values from N.B.S. circular 499. ⊙ Ranges of beta-rays measured by the authors; energies are the best accepted values from N.B.S. circular 499. ⊡ Ranges of beta-rays from $B^{12}$ (range—Hereford and Swann, energy—Fowler, Lauritsen, and Lauritsen) and $N^{12}$ (Alvarez). —●— Two practical range points due to Bleuler and Zunti. × Practical range measurements from Hereford and Swann. The solid line represents the empirical equation $R=412\ E_0^{1.265-0.0954\ln E_0}$ and is a good fit below 2.5 Mev. The dashed line represents the Feather relation $R=530\ E_0-106$ and is a good fit above 2.5 Mev.

are compatible, then range energy measurements made in various laboratories should agree.

If interfering effects such as conversion electrons and Compton electrons are not present, then range determinations should not depend upon geometry or detector sensitivity to any great extent. For example, in the case of $Cu^{62}$, suppose it is possible to discriminate against the gamma-ray background down to 95 percent of the range. Then increasing the detector sensitivity by a factor of forty will only make it possible to measure to 98 percent of the range; a 3 percent increase for a fortyfold increase in detector sensitivity. Not all spectra decrease as rapidly in intensity near the end point, but the decrease is always sufficiently rapid to allow direct comparison of the results taken with different detectors under diverse experimental arrangements. Furthermore, since the beta-ray beam is completely diffuse near the range thickness, the shape of the absorption curve in this region will not be a strong function of counting geometry. This is discussed further in a later section.

Range-energy points obtained by Varder,[14] Schonland,[15] Madgwick,[16] Eddy,[17] and Marshall and Ward[18] for homogeneous electrons; Widdowson and Champion,[19] Moore,[20] Glendenin,[7] and the authors, for beta-rays are summarized in Table I and are plotted in Fig. 2. The figure also includes two points for homogeneous electrons ($R_p$) as given by Bleuler and Zunti,[11] and the following ranges in the energy region above 2 Mev: the 13.43 Mev[21] point of $B^{12}(R_\beta)$ as measured by Hereford,[22] the series of points ($R_p$) between 3 and 12 Mev measured by Hereford and Swann,[12] the 16.6-Mev point ($R_\beta$) of $N^{12}$ measured by Alvarez,[23] and the two points due to Trump, Wright, and Clarke.[24]

The energies of the homogeneous electrons were determined either from an accelerating potential (Schonland) or from magnetic spectrometer measurements. The end-point energies of the beta-rays given in Table I were determined by spectrometer measurements and are listed in N.B.S. Circular 499.[25]

In the case of $N^{12}$ the end-point energy was calculated from the known $C^{12}(p, n)$ threshold.

[14] R. W. Varder, Phil. Mag. **29**, 725 (1915).
[15] V. F. J. Schonland, Proc. Roy. Soc. (London) **A104**, 235 (1923).
[16] E. Madgwick, Proc. Cambridge Phil. Soc. **23**, 970 (1927).
[17] C. E. Eddy, Proc. Cambridge Phil. Soc. **25**, 50 (1929).
[18] J. S. Marshall and A. G. Ward, Can. J. Research **15**, 39 (1937).
[19] E. E. W. Widdowson and F. C. Champion, Proc. Phil. Soc. (London) **50**, 185 (1938).
[20] B. L. Moore, Phys. Rev. **57**, 355 (1940).
[21] W. F. Hornyak and T. Lauritsen, Phys. Rev. **77**, 160 (1950).
[22] F. L. Hereford, Phys. Rev. **74**, 574 (1948).
[23] L. Alvarez, Phys. Rev. **75**, 1815 (1949).
[24] Trump, Wright, and Clarke, J. Appl. Phys. **21**, 345 (1950).
[25] N.B.S. Circular 499, "Nuclear data," U. S. Department of Commerce.

TABLE I. Values used in Fig. 2, the ranges are from the references indicated and the energies are from N.B.S. circular 499.

| Author | Method of determining range | Emitter | Energy (Mev) | Range (mg/cm²) | Reference |
|---|---|---|---|---|---|
| Varder | Extrapolation, $R_p$ | Homogeneous rays | See reference | | 14 |
| Schonland | Extrapolation, $R_p$ | Homogeneous rays | See reference | | 15 |
| Madgwick | Extrapolation, $R_p$ | Homogeneous rays | See reference | | 16 |
| Eddy | Extrapolation, $R_p$ | Homogeneous rays | See reference | | 17 |
| Marshall and Ward | Extrapolation, $R_p$ | Homogeneous rays | See reference | | 18 |
| Trump | Extrapolation, $R_p$ | Homogeneous rays | 2.00 | 966 | 24 |
| | Extrapolation, $R_p$ | Homogeneous rays | 3.00 | 1540 | |
| Widdowson and Champion | $W$ and $C$, $R_\beta$ | $Bi^{212}$(ThC) | 2.25 | 1023 | 19 |
| | $W$ and $C$, $R_\beta$ | $Mg^{27}$ | 1 80 | 885 | |
| | $W$ and $C$, $R_\beta$ | $As^{76}$ | 3.12 | 1454 | |
| | $W$ and $C$, $R_\beta$ | $As^{76}$ | 2.56 | 1384 | |
| Moore | Sargent, $R_\beta$ | $Na^{24}$ | 1.39 | 621 | 20 |
| | Sargent, $R_\beta$ | $Mg^{27}$ | 1.80 | 821 | |
| | Sargent, $R_\beta$ | $P^{32}$ | 1.71 | 810 | |
| | Sargent, $R_\beta$ | $Rh^{104}$ | 2.6 | 1198 | |
| | Sargent, $R_\beta$ | $C^{11}$ | 0.98 | 447 | |
| | Sargent, $R_\beta$ | $N^{13}$ | 1.24 | 557 | |
| Glendenin | Inspection, $R_\beta$ | $Ra^{228}$ | 0.053 | 6 | 7 |
| | Inspection, $R_\beta$ | $Rb^{87}$ | 0.13 | 20 | |
| | Feather, $R_\beta$ | $Nb^{95}$ | 0.146 | 30 | |
| | Inspection, $R_\beta$ | $Lu^{176}$ | 0.22 | 48 | |
| | Feather, $R_\beta$ | $Co^{60}$ | 0.31 | 81 | |
| | Feather, $R_\beta$ | $Zr^{95}$ | 0.400 | 122 | |
| | Feather, $R_\beta$ | $I^{131}$ | 0.600 | 213 | |
| | Feather, $R_\beta$ | $Sb^{124}$ | 0.65 | 254 | |
| | Feather, $R_\beta$ | $Ba^{140}$ | 1.022 | 426 | |
| | Feather, $R_\beta$ | $Cd^{115}$ | 1.13 | 527 | |
| | Feather, $R_\beta$ | $Sr^{89}$ | 1.50 | 741 | |
| | Feather, $R_\beta$ | $Te^{129}$ | 1.80 | 812 | |
| | Feather, $R_\beta$ | $Y^{90}$ | 2.18 | 1065 | |
| | Inspection, $R_\beta$ | $Pa^{234}$ | 2.32 | 1105 | |
| | Feather, $R_\beta$ | $Sb^{124}$ | 2.37 | 1220 | |
| | Feather, $R_\beta$ | $Pr^{144}$ | 3.07 | 1575 | |
| Katz and Penfold | $n$th power, $R_\beta$ | $Cu^{62}$ | 2.92 | 1440 | |
| | $n$th power, $R_\beta$ | $Na^{24}$ | 1.390 | 601 | |
| | $n$th power, $R_\beta$ | $Rh^{106}$ | 3.55 | 1770 | |
| | $n$th power, $R_\beta$ | $Rh^{106}$ | 2.30 | 1080 | |
| | $n$th power, $R_\beta$ | $Au^{198}$ | 0.97 | 399 | |
| | $n$th power, $R_\beta$ | $Mn^{56}$ | 2.86 | 1440 | |
| | $n$th power, $R_\beta$ | $Mn^{56}$ | 1.05 | 462 | |
| | $n$th power, $R_\beta$ | $Mn^{56}$ | 0.73 | 277 | |
| | $n$th power, $R_\beta$ | $Be^{10}$ | 0.555 | 181 | |
| | $n$th power, $R_\beta$ | $Bi^{210}$(RaE) | 1.17 | 508 | |

Each of the authors whose beta-ray ranges are listed in Table I has used a different method of absorption curve analysis. These methods will be discussed later. The ranges by Glendenin, using the Feather method of analysis appear to be based on a range of 502 mg/cm² for RaE (1.17 Mev). Since the Feather method gives ranges relative to RaE, the published values of Glendenin have been corrected to our value of 508 mg/cm².[26] No correction was necessary in the case of Moore's ranges since they are based on Sargent's value of 510 mg/cm² for RaE[30].

Two facts are immediately evident from Fig. 2. One is that there is no discernible difference in the ranges of homogeneous electrons and beta-particles. Therefore it seems that the definition of the practical range ($R_p$) in the case of homogeneous electrons is compatible with the range of beta-rays ($R_\beta$) as determined by using one of the methods of absorption curve analysis. (A more quantitative analysis of this point is given in the discussion of Eq. (8).) The second is that there seems to be no discernible difference in the ranges of positron and electron spectra. This was to be expected since annihilation of positrons in flight is very rare. Further, there seems to be compatibility between the various methods of absorption curve analysis.

Feather[6] suggested that the range-energy relation may be represented by the following equation over a limited range of the variables involved

$$R = AE_0 - B, \tag{1}$$

where $R$ is the range in mg/cm² and $E_0$ is the energy in Mev for the case of homogeneous electrons, or the end-point energy in the case of a beta-spectrum. Feather gave the values $A=543$ and $B=160$ for the constants. Since then there have been many other values suggested. Some of these are collected in Table II, and

[26] The authors would like to thank B. W. Sargent, J. D. Hughes, and H. D. Evans for making available to them absorption curves of RaE. These curves, taken in different laboratories, gave ranges within a few mg/cm² of each other and lead to an average value of 508 mg/cm² for the range of RaE betas.

TABLE II. Table of values for $A$ and $B$ ($R$ in mg/cm² and $E_0$ in Mev).

| Source | $A$ | $B$ |
|---|---|---|
| Feather[a] | 543 | 160 |
| Widdowson andChampion[b] | 536 | 165 |
| Bleuler and Zunti[c] | 571 | 161 |
| Science and Eng. of N.P.[d] | 540 | 150 |
| Glendenin and Coryell[e] | 542 | 133 |
| Sargent[f] | 526 | 94 |
| Katz and Penfold | 527 | 112 |

[a] See reference 27.
[b] See reference 19.
[c] See reference 11.
[d] See reference 28.
[e] See reference 29.
[f] See reference 30.

they are to apply to the energy range 0.8 Mev to 3.0 Mev. Feather showed that the work of Varder could be represented with $A=469$, $B=71$ and that of Madgwick with $A=552$, $B=97$.

From an examination of Fig. 2 the authors have found the values for $A$ and $B$ as listed in the table. However, the relation between the energy and the range does not appear to be exactly linear in the region 0.8 to 3.0 Mev so these values can only be regarded as approximate.

At low energies the rate of change of the velocity of an electron travelling through aluminum has been represented by [31,32]

$$-d\beta/dx=2.2/\beta^3 \quad 0.1<\beta<0.6, \tag{2}$$

where $\beta$ is $v/c$ and $x$ is measured in cm and so the range is proportional to the square of the energy. At larger values of $\beta$ the range becomes proportional to the first power of the energy as is expressed in the Feather formula. In view of these considerations Flammersfeld[33] was led to suggest that the range-energy relation has a hyperbolic form and can be represented by

$$(R+a)^2/a^2-E_0^2/b^2=1. \tag{3}$$

He has evaluated the constants and gives the following formula for the relation between the end-point energy of a beta-ray spectrum and the maximum range:

$$E(\text{Mev})=1.92(R_0^2+0.22R_0)^{\frac{1}{2}} \quad (R_0 \text{ in gm/cm}^2). \tag{4}$$

In order to obtain the values of the constants in (4), Flammersfeld made use of the range-energy values for a number of beta-ray spectra with end-point energies between 0.09 and 3.0 Mev, as well as the maximum ranges given by Schonland and Varder (values referring to work by Schonland and Varder in Table I are values of the practical range).

[27] N. Feather, Proc. Cambridge Phil. Soc. **34**, 599 (1938).
[28] *The Science and Engineering of Nuclear Power VI* (Addison-Wesley Press, Cambridge, Massachusetts, 1947).
[29] L. E. Glendenin and C. D. Coryell, MDDC 19 (1946).
[30] B. W. Sargent, Can. J. Research **A17**, 82 (1939).
[31] F. Rasetti, *The Elements of Nuclear Physics* (Prentice Hall, Inc., New York, 1936).
[32] B. W. Sargent, Trans. Roy. Soc. Can. **22**, Sec. 3, 179 (1928).
[33] A. Flammersfeld, Z. Naturforsch. **2a**, 370 (1947).

Glocker[34] has re-evaluated the constants in (4) on the basis of the values of $R_p$ given by Schonland and Varder and obtained

$$E(\text{Mev})=2.1(R_p^2+0.13R_p)^{\frac{1}{2}} \quad (R_p \text{ in gm/cm}^2). \tag{5}$$

He compares the range-energy values obtained from this equation with those obtained by integration of a theoretical formula giving the rate of energy loss resulting from ionizing collisions. The agreement is good from 4 to nearly 100 Mev.

Several roughly straight line portions are evident in the data plotted in Fig. 2. For this reason a number of authors have proposed a relation between range and energy of the form $R=aE_0^n$. For the constants: Glocker[34] has proposed $a=710$, $n=1.72$ in the energy range 0.001 to 0.3 Mev.; Glendenin and Coryell[29] have proposed $a=407$, $n=1.38$ in the energy range 0.15 to 0.8 Mev; and Libby[35] has proposed $a=667$, $n=1.66$ in the energy range 0.05 to 0.15 Mev.

In order to represent the data in Fig. 2, the authors have let $n$ be variable and have used the equation

$$R(\text{mg/cm}^2)=aE_0^{(b-c\ln E_0)}=aE_0^n. \tag{6}$$

From the experimental points the value of $R$ at $E_0=1$ was chosen as 412. The value of $n$ was then determined for each of the experimental points shown in Fig. 2. These values of $n$ were then plotted against $\ln E_0$. The best straight line through the data gave

$$n=1.265-0.0954\ln E_0. \tag{7}$$

The final equation for the range-energy relations was thus

$$R(\text{mg/cm}^2)=412E_0^{1.265-0.0954\ln E_0}, \tag{8}$$

where the energy is in Mev. A plot of this equation is shown in Fig. 2 as the solid line. It is seen that a remarkable fit to the experimental values is obtained for energies up to about 3 Mev.†

TABLE III.

| | $u_0$ | $u_1$ | $u_2$ |
|---|---|---|---|
| Average of beta-ray points (35 points) | −0.05% | 4.1% | 5.1% |
| Average of monoenergetic electron points (59 points) | +0.08% | 4.1% | 5.8% |

[34] R. Glocker, Z. Naturforsch. **3a**, 129 (1948).
[35] W. E. Libby, Anal. Chemie. **19**, 2 (1947).

† *Note added in proof:*—Dr. S. Ecklund of the Swedish atomic energy project has kindly transmitted to the authors range-energy measurements by Dr. Ingvar Carlvik using monoenergetic electrons. His results and their agreement with Eq. (8) are summarized below.

| Energy Mev | Range Measured | Range Calculated |
|---|---|---|
| 0.100 | 13 ±0.5 | 13.4 |
| 0.124 | 19.5±0.5 | 19.5 |
| 0.149 | 25 ±0.5 | 26.4 |
| 0.174 | 33 ±0.5 | 33.8 |
| 0.199 | 41.5±0.5 | 41.6 |

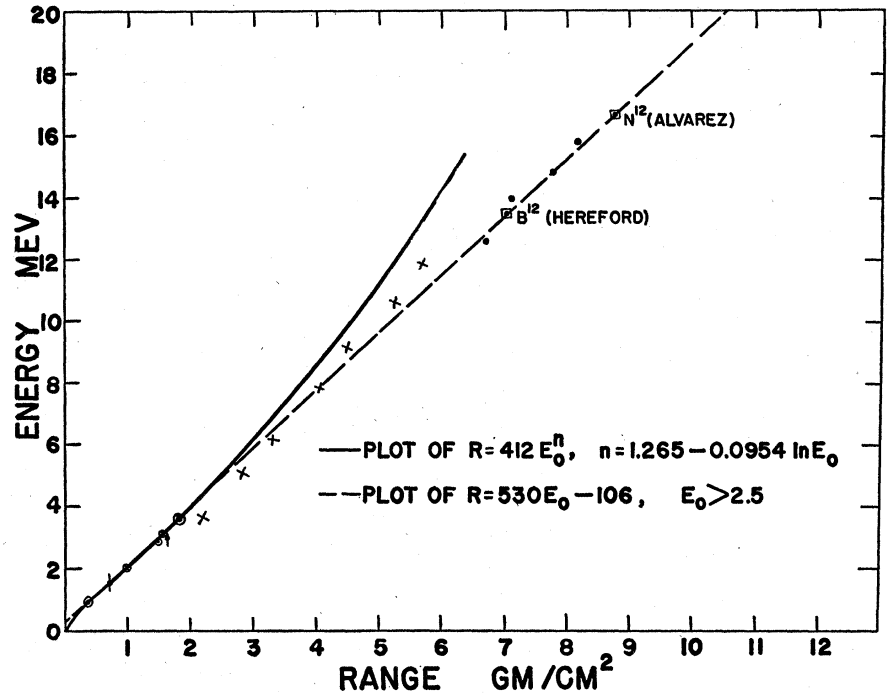


FIG. 3. Range-energy curve plotted on a linear scale to emphasize the high energy region. Points represented by ×, ⊙, and ⊗ are the same as given in Fig. 2. The solid and dashed lines are also drawn in Fig. 2. ● Practical ranges as measured in this laboratory by Johns *et al.*

In order to get a "measure" of the goodness of fit of the experimental points below 3 Mev to our Eq. (8), we define

$$\delta=(E_{\text{expr}}/E_{\text{equ}}-1),$$

where $E_{\text{equ}}$ comes from (8) and $E_{\text{expr.}}$ from Table I. The fit may then be measured by

$$u_0=1/N\sum_1^N \delta_i$$

and the mean deviation and standard deviation by

$$u_1=1/N\sum_1^N |\delta_i|$$

$$u_2=[1/N\sum_1^N |\delta_i|^2]^{\frac{1}{2}}.$$

Table III summarizes our results.

In the region 0.15 to 0.8 Mev the value of $n$ varies from 1.42 to 1.39 with a mean value of 1.36 in good agreement with the exponent used by Glendenin and Coryell; the agreement with Libby and Glocker is not so good. In Table IV we have collected the nuclides whose ranges have been determined by the method of absorption curve analysis proposed by the authors, and have compared the energies obtained from relation (8) with those listed in the N.B.S. Circular 499.[25] The absorption curves for $Cu^{62}$, $Na^{24}$, $Au^{198}$, and $Mn^{56}$, were experimentally determined by us.

Equation (8) deviates from the experimental data in the region above 3 Mev. This high energy region has been replotted to a linear scale in Fig. 3.

All the plotted points are from the absorption of continuous spectra except those of Hereford and Swann[12] (represented by crosses in Fig. 3), the two points by Trump, Wright, and Clarke,[24] and four points taken in this laboratory with monoenergetic electrons extracted from our betatron.[36] The Hereford and Swann points were obtained by selectring a group of beta-rays from the $B^{12}$ spectrum by magnetic means and then obtaining an aluminum absorption curve through the use of a triple-double coincidence method.

The point representing $N^{12}$ should be quite accurate since the range was well determined and the decay energy (end-point energy) was obtained by a simple calculation from the $C^{12}(p,n)$ threshold which was measured by Alvarez.[23] In order to measure this thresh-

TABLE IV. Comparison of energies from range-energy relation (8) and magnetic spectrometer measurement for nuclides investigated by the authors. (Note $Rh^{106}$ energies given in discussion of Fig. 13.)

| Emitter | Range (mg/cm²) | Energy (Mev) Magnetic spectrometer | Energy (Mev) Range-energy equation (8) | % diff. |
|---|---|---|---|---|
| $Cu^{62}$ | 1440 | 2.92 | 2.91 | −0.3 |
| $Na^{24}$ | 601 | 1.390 | 1.370 | −2 |
| $Rh^{106}$ | 1770 | 3.55 | 3.52 | −1 |
| $Rh^{106}$ | 1080 | 2.30 | 2.25 | −2 |
| $Au^{198}$ | 399 | 0.97 | 0.97 | 0 |
| $Mn^{56}$ | 1440 | 2.86 | 2.91 | +1 |
| $Mn^{56}$ | 462 | 1.05 | 1.09 | +4 |
| $Mn^{56}$ | 277 | 0.73 | 0.73 | 0 |
| $Be^{10}$ | 181 | 0.555 | 0.531 | −4 |
| $Ba^{140}$ | 405 | 1.022 | 0.98 | −4 |
| RaE | 508 | 1.17 | 1.18 | +1 |

[36] Johns, Cunningham, and Katz, Phys. Rev. 83, 952 (1951).

old he used a well-substantiated proton range-energy curve.

The points $N^{12}$, $B^{12}$, $Rh^{106}$, $Cu^{62}$, and $Au^{198}$, the four points taken in this laboratory, and those due to Trump, Wright, and Clarke form a straight line. This is the line shown dashed in Fig. 3. It is seen that the points of Hereford and Swann cross this line and that Eq. (8) (solid curve) deviates sharply from it.

The authors propose that the range-energy curve in the region of energies between 2.5 and 20.0 Mev be represented by a Feather formula. Matching such a formula to (8) in both value and slope at 2.5 Mev, the relation obtained is

$$R(\text{mg/cm}^2)=530E_0(\text{Mev})-106 \quad (2.5<E_0<20.0). \quad (9)$$

In the intermediate energy range (1 to 8 Mev) Fowler, Lauritsen, and Lauritsen[37] have used a formula originally due to Bohr:

$$R=aE_0(E_0+m_0c^2)/(E_0+2m_0c^2). \quad (10)$$

The values of the constant $a$ are adjusted to the type of range under consideration, thus with the range measured in mg/cm² and $E_0$ and $m_0^2c$ in Mev, they give $a=648$ for $R_0$, 594 for $R_p$, and 566 for $R_\beta$ (private communication). We find the value $a=555$ to give the best fit in the region of 1 to 8 Mev for both $R_p$ and $R_\beta$.

Some measurements have also been reported on the range of secondary electrons which result when a converter, generally aluminum, is irradiated with monochromatic gamma-rays. In this case the range is very difficult to define. Usually the range $R_n$ is given as the thickness of aluminum necessary to reduce the initial electron intensity by a factor $2^n$. Fowler, Lauritsen, and Lauritsen[37] have published values of $R_n$ for a number of energies and give graphs for range, with $n$ varying from 1 to 8 as well as for $n=\infty$. The most recent values[38] of $R_7$ for the 7.4-Mev $Be^9(p,\gamma)$ secondaries is 340 mg/cm² and for the 17.6-Mev $Li(p,\gamma)$ secondaries is 824 mg/cm². Ageno and Chiozzotto[39] have also published values of $R_{1/2}$, $R_{1/20}$, and $R_{1/100}$ for the $Li(p,\gamma)$ secondaries in aluminum. These values differ considerably from the curves of reference.[37]

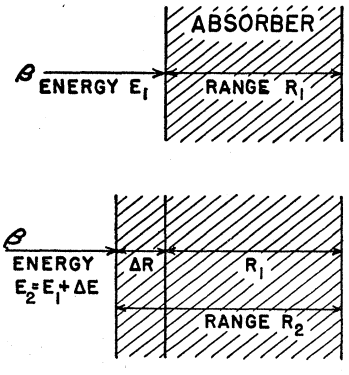


FIG. 4. Diagram to illustrate how range varies with change of electron energy.

It is of some interest to compare $(dE_0/dR)$ from (8) and (9) to the rate of loss of energy by ionization as predicted by the theoretical equation given by Heitler.[40]

$$\left(-\frac{dW}{dx}\right)_{\text{coll.}}=\tfrac{3}{4}NZ\mu\varphi/\beta^2 \times[\ln(W-\mu)W^2\beta^2/2\mu(ZI)^2+(\mu/W)^2]. \quad (11)$$

The notation is that of Heitler except that the total energy is designated by $W$ so as not to confuse it with the kinetic energy $E$. Differentiating (8) and (9) one obtains

$$(dE_0/dR)=(E_0/R)(1.265-0.191\ \ln E_0)^{-1} \quad \text{for} \quad E_0\leqslant 2.5\cdots \quad (12)$$

$$(dE_0/dR)=0.00189 \quad \text{for} \quad E_0\geqslant 2.5. \quad (13)$$

Strictly speaking, $dx$ in (11) is the increase in path length when the electron energy is increased by $dW$, whereas $dR$ is the corresponding increase in the range. However, since the range is a measure of the paths of those electrons which have suffered only very small deviations, then we would expect $dR$ to be nearly equal to $dx$. Wang[41] has criticized the use of the rate of change of range with energy as an indication of the ionization loss of energy by electrons. In support of his arguments he presents a diagram (Fig. 4 of reference 41) to show that $(\Delta E_0/\Delta R)$ is in fact not equal to $(\Delta E_0/\Delta x)$. Instead of this diagram one should examine the problem from the following point of view; let us suppose that for all practical purposes all electrons of initial energy $E_1$ are absorbed at the end of the range $R_1$. Electrons with initial energy $E_2=E_1+\Delta E$ will lose energy $\Delta E$ in traveling $\Delta R=R_2-R_1$, and then will travel a further distance $R_1$ before being completely absorbed. These quantities are illustrated in Fig. 4. An electron of energy $E_2$ will lose $\Delta E$ in traveling $\Delta R$. In the limit the rate of energy loss is $(dE_0/dR)$.

Equations (11), (12), and (13) are plotted in Fig. 5. The rate of change of energy with range, $(dE_0/dR)$, is larger than that predicted by the theoretical equation for energy loss by ionization alone for energies less than about 20 Mev. Over the major portion of the region from 0.01 to 20 Mev the "range-energy" loss is about 25 percent greater. The decrease in energy loss above one Mev when the polarizability of the medium is taken into account as indicated by Fermi[42] and by Halpern and Hall[43] has been applied to the computations from Eq. (11).

The discrepancy between the two energy loss curves is difficult to explain. The following facts are pertinent

[37] Fowler, Lauritsen, and Laruitsen, Revs. Modern Phys. **20**, 265 (1948).

[38] The authors would like to thank Dr. W. A. Fowler for communicating these values to them.

[39] M. Ageno and M. Chiozzotto, Nuovo cimento **6**, 81 (1949).

[40] W. Heitler, *The Quantum Theory of Radiation* (Oxford University Press, London, 1936), p. 219.

[41] T. J. Wang, Nucleonics **7**, 55 (1950).

[42] E. Fermi, Phys. Rev. **57**, 485 (1940).

[43] O. Halpern and H. Hall, Phys. Rev. **73**, 477 (1948).

to this discussion though they do not seem to remove the discrepancy.

(a) The energy loss $\Delta E$, used in the discussion of Fig. 4 was not specified too clearly. Equation (11) gives the *average* rate of energy loss. A number of papers have recently appeared[44,45] emphasizing the need for using the *most probable* energy loss as calculated by Landau.[46] The most probable energy loss for a given foil thickness, as illustrated by the graph of Warshaw and Chen, is even less than the average energy loss and so does not give better agreement with our $(dE_0/dR)$ curve.

(b) In Fig. 4 comparison is made between the range $R_1$ of electrons of initial energy $E_1$ and the residual range of electrons of initial energy $E_1+\Delta E$ after traversing a foil thickness $\Delta x$. This comparison is open to some doubt since in one case we have a parallel beam of monoenergetic electron of energy $E_1$, while in the second case on traversing $\Delta x$ of foil the most probable energy is $E_1$, though electrons with greater and smaller energy are present and the electrons are now traveling in all directions. Under these conditions the residual range may be greater than $R_1$ because some electrons with energies greater than $E_1$ are present, or less than $R_1$ because of scattering. Since the observed $(dE_0/dR)$ is too large, one might then conclude that scattering effects are most important.[47] Such a conclusion would imply that range measurements are strongly dependent on experimental geometry, this is contrary to the fact that ranges measured in different laboratories are compatible.

So far, no account has been taken of the effects of radiation losses on the range. These losses will not become appreciable until the probability for loss by radiation is approximately equal to the probability for loss by ionization (around 52 Mev for aluminum). In any case, large radiation losses are only suffered by a small number of electrons and so the effect on the range should be small. Radiation losses will tend to increase $(dW/dx)$ over that given by (11) and so make the variance between experiment and theory in the high energy range even greater.

A theoretical range can be defined from the theoretical rate of energy loss formula (11) to be

$$R_t=\int_{W_0}^{\mu} dW/(dW/dx), \tag{14}$$

where $\mu=m_0c^2$. This range will be the average trajectory length or the *average true range*.[33] Such a range could be measured with the help of a Wilson cloud chamber or nuclear emulsion. The relation between $R_t$ and $R_0$ might be expressed in the form

$$R_0=R_t\phi(E_0, S, G), \tag{15}$$

where $\phi$ is a function of the initial energy, the detector

[44] S. D. Warshaw and J. J. L. Chen, Phys. Rev. **80**, 97 (1950).
[45] O. Blunck and S. Leisegang, Z. Physik **128**, 500 (1950).
[46] L. Landau, J. Phys. (USSR) **8**, 201 (1944).
[47] The authors would like to thank Dr. T. Lauritsen for pointing out this fact to them.

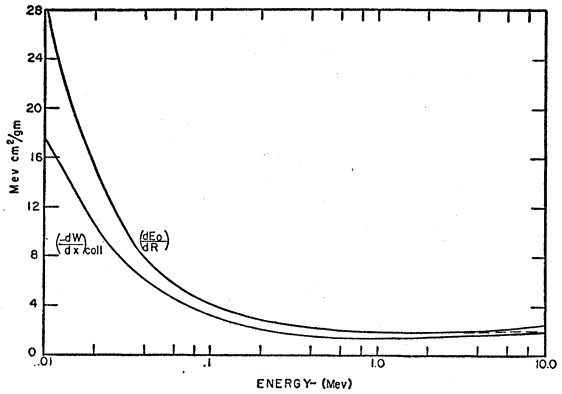


FIG. 5. Rate of change of energy with range $(dE_0/dR)$ computed from the empirical Eqs. (12) and (13) compared with the rate of energy loss for electrons by ionization $(-dW/dx)_{\text{coll}}$ according to the theoretical Eq. (11).

sensitivity, and the geometry. In particular, no electron can penetrate to the maximum range without suffering some scattering, and so $\phi$ will contain a function of the cosine of some minimum average scattering angle referred to the forward direction. Thus, while the equivalence of trajectory and maximum range cannot hold exactly, $R_0$ may be very nearly equal to $R_t$.

The integration expressed by (14) has been carried out by Fowler, Lauritsen, and Lauritsen[37] by reducing Eq. (11) to the extreme relativistic case. Since the reduction of (11) is only valid down to about 3 Mev, the results are expressed in terms of some standard range.

Hereford and Swann[12] have integrated (14) and taken into account multiple scattering. To do this two reference points are needed, and they chose the two points by Bleuler and Zunti shown in Fig. 2 and Fig. 3.

For approximate computations of the absorption of nuclear beta-rays it has been customary for some workers[48,49] to assume that over a limited region the intensity of the beam varies exponentially with absorber thickness,

$$I=I_0\exp[-\mu x/\rho], \tag{16}$$

where $\mu/\rho$ is an apparent mass absorption coefficient expressed in $cm^2/mg$ and $x$ is the absorber thickness in $mg/cm^2$.

This equation may be related to the range-energy curve through the following analytical, though experimentally unrealistic formulation. Suppose the range is defined in principle as that thickness which reduces the initial intensity $I_0$ to some small fraction $kI_0$, where $k$ is a small number of the order of $10^{-4}$ or less depending on the sensitivity of the detector and the energy of the beta-rays involved.

Then

$$k=\exp[-\mu R/\rho]$$

or

$$\mu/\rho=-\ln k/R=-\ln k/aE_0^n. \tag{17}$$

[48] See N. Feather, British Report BDDA 161, 504 (1944).
[49] R. E. Lapp and H. L. Andrews, *Nuclear Radiation Physics* (Prentice-Hall, Inc., New York, 1948), p. 179.

Evans,[50] Siri,[51] and the Science and Engineering of Nuclear Power[28] give the equation[52]

$$\mu/\rho = 22/E_0^{1.33} \tag{18}$$

for energies between 0.1 and 3.0 Mev.

In the energy interval involved, the $n$ value given by Eq. (8) varies from 1.16 to 1.48 having an average value of 1.32 which is in excellent agreement with the exponent used by Evans. The constant in the equation corresponds to the assumption that $k=10^{-4}$. Gleason, Taylor, and Tabern[53] have recently published a similar equation for the mass absorption coefficient. In the energy interval 0.15 to 3.5 Mev they give $\mu/\rho = 17/E_0^{1.43}$.

## METHODS FOR DETERMINING THE RANGE

### Inspection Method

This method is the simplest and perhaps the least reliable. The range is determined from an inspection of the absorption curve. In order to find where the curve meets the background many accurate experimental points are required close to the range thickness. If the curve approaches the background very slowly, then it is difficult to obtain good accuracy. Thick sources tend to have an overabundance of slow electrons because of self-absorption, thus giving rise to this difficulty. Hence thick sources should be avoided. A high gamma-ray background will also cause the gradual merging of the absorption curve and the background. In this case there is little one can do.

### Feather Method

Feather[27] suggested that the absorption curve of some activity whose range is known could be used as a standard for comparing to an absorption curve whose range is to be determined. He used RaE as the standard. The absorption curve of RaE (with background subtracted) is divided into ten equal parts along the axis of filter thickness. These thicknesses are designated

$$d_n{}^0 = R_0/n \quad (n=1, 2, 3, \cdots 10),$$

where $R_0$ is the range of RaE.

The corresponding intensities are $I_n{}^0$. The ordinate of the unknown absorption curve (intensity) is divided into ten parts $I_n$, such that $I_n = I_n{}^0$. If the thickness corresponding to $I_n$ is $d_n$, then Feather assumed that

$$d_n/d_n{}^0 \rightarrow R/R_0 \quad \text{for} \quad n \rightarrow 10, \tag{19}$$

where $R$ is the range of the unknown.

For this method to be valid the unknown and standard must become similar at least in an asymptotic fashion as the end point is approached. This is the main weakness of the method. The use of RaE as a standard was a poor choice since its beta-spectrum contains more low energy electrons than are ordinarily found in an allowed spectrum. The absorption curve thus exhibits a long high energy tail.

Apart from the exact choice of a standard, there is little reason to expect that all absorption curves will have the same shape, even under identical experimental conditions. Some of the factors which effect the absorption curve shape are as follows:

1. Selection rule for the transition involved.
2. Source thickness (variation with energy and atomic number).
3. Backscattering (variation with atomic number and energy).
4. Conversion electrons.
5. Compton electrons and photoelectrons.
6. Counter efficiency (variation with energy).
7. Atomic number (in Fermi theory).
8. Whether negative or positron emission.
9. End-point energy (in Fermi theory).

In spite of these criticisms, the Feather method has given fairly accurate results. Many values of end-point energy which were originally obtained by this method have been substantiated by subsequent magnetic spectrometer measurements. The chief merit of the Feather method is that it readily yields a range which is more reliable than one obtained by inspection.

### Sargent Method

Quite independent of Feather, and at about the same time, Sargent[30] published a method of analysis which also makes use of a standard absorption curve with which the unknown curve is compared.

Sargent found that the absorption curves of RaE and $UX_2$ were similar in shape for absorber thicknesses greater than about half their ranges. He showed that a plot of the logarithm of the intensity $I$ *versus* $x$, the fractional range, resulted in coincidence of the two curves for $x>0.5$.

In applying Sargent's method an approximate value of $R$ is obtained by inspection of the absorption curve of the unknown spectrum. This value is then adjusted until the corresponding values of $(\log I - \log I_{\text{std}})$ have a constant difference for all values of $x$; or, if that is not possible, for all values of $x$ greater than some minimum value.

There is little to choose between the Feather and Sargent methods, though in some instances Feather's method is somewhat simpler to apply. When the unknown and the standard differ greatly in shape Feather's method may give a value by extrapolating the curve of $d_n/d_n{}^0$ *vs* $n$, while in this case the Sargent method may not be applicable.

Moore[20] has used the Sargent method to obtain the ranges listed in Table I. Recently, Evans[54] applied the Sargent method to the absorption curves of RaE, AcC″, and $Tl^{204}$. He found the AcC″ coincides with RaE for

[50] Biological and Medical Physics (Academic Press, Inc., New York, 1948), Vol. 1, p. 163.

[51] W. E. Siri, *Isotopic Tracers and Nuclear Radiations* (McGraw-Hill Book Company, Inc., New York, 1949), p. 58.

[52] This equation probably stems from an article by G. Fournier, Ann. phys. **8**, 905 (1927) in which it is shown that the mass absorption coefficient for RaE, UX, and RaC beta-rays can be represented by $\mu/\rho = (0.169/E_0^{1.33})(105+Z)$.

[53] Gleason, Taylor, and Tabern, Nucleonics **8**, 12 (1951).

[54] H. D. Evans, Proc. Phys. Soc. (London) **63**, 575 (1950).

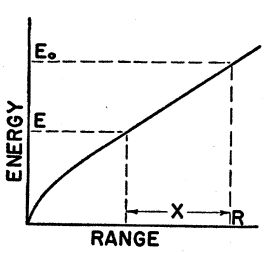


FIG. 6(a). Relation between electron energy $E$ and filter thickness $x$ for a given initial energy $E_0$ as obtained from a range-energy curve.

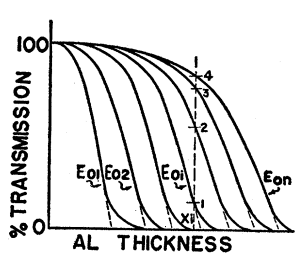


FIG. 6(b). Absorption curves for electrons of initial energies $E_{01}$, $E_{02}$, $\cdots E_{0i}$, $\cdots E_{0n}$ as computed by Bleuler and Zunti. Vertical dashed line indicates the fraction of electrons with indicated energies which pass through an absorber of a given thickness.

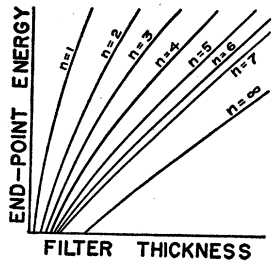


FIG. 6(c). Absorption curves as computed by Bleuler and Zunti for Fermi allowed spectra. Each line shows the thickness of absorber necessary to give a fractional transmission $1/2^n$ as a function of the end-point energy.

$x>0.65$, and thallium with RaE for $x>0.45$. As was to be expected, this analysis gave the same ranges for AcC″ and $Tl^{204}$ as found by the Feather method, when based on a fixed range for RaE.

### Method of Bleuler and Zunti

These workers[11] developed a set of curves which were designed to overcome the objections to the use of RaE as a standard in the Feather method.

Bleuler and Zunti set themselves the task of obtaining a set of absorption curves for Fermi allowed spectra.[4] The exact shape of a spectrum depends on the end-point energy $E_0$, the atomic number $Z$ of the residual nucleus, and whether positrons or electrons are emitted, so curves for different combinations of values of these variables could be plotted. Bleuler and Zunti chose to plot a set of curves for $Z$ fixed and different values of $E_0$, and allow for variations in $Z$ and the type of radiation through separate correction curves.

The procedure by which the absorption curves were obtained may be summarized as follows: according to Bothe,[55] the fraction $N/N_0$ of the initial intensity left in a homogeneous beam of electrons (initial energy $E_0$) after traversing a distance $x$ through a thick absorber (complete diffuse radiation) is

$$N/N_0=\exp\left[-\int_0^x \alpha(x)dx\right] \tag{20}$$

$$\alpha(x)=14.2[E+0.511/E(E+1.022)]^2 \text{ cm}^{-1}, \tag{21}$$

where $E$ is the energy in Mev of the electrons after passing through a thickness $x$. Bleuler and Zunti assume that for a given $E_0$, $E$ and $x$ may be related through a range-energy curve ($R_p$ *vs* $E_0$) as indicated in Fig. 6(a). Graphical integration of Eq. (20) yielded absorption curves for incident energies $E_{01}$, $E_{02}$, etc. The sketch of Fig. 6(b) illustrates these curves. They may also be plotted in a manner similar to Fig. 1(c). The ordinates give the fraction by which a beam of incident energy $E_{0n}$ is reduced in intensity after passing through an absorber of thickness $x$.

Bleuler and Zunti next plotted the Fermi equation for allowed transitions with maximum energies of 1, 2, 3, 5, and 10 $m_0c^2$, and $Z=0$, 20, 40, and 90 as well as for positron disintegration with $Z=40$. A particular Fermi curve was chosen and a particular value of filter thickness, $x_i$. Each point on the Fermi curve was multiplied by the appropriate value of $N/N_0$ from (20) (called $1, 2, 3\cdots$ in Fig. 6(b)). The area under the resulting distorted spectrum curve gave the fraction of betas passing through the absorber thickness $x_i$. The process was repeated for different thicknesses of absorber until a complete absorption curve was obtained for each of the Fermi curves.

Bleuler and Zunti then divided the ordinates of these absorption curves into intensities with fractions $1/2^n$ ($n=1, 2, 3, \cdots$) of the initial intensity. Their standard absorption curves are illustrated schematically in Fig. 6(c).

An unknown absorption curve is analyzed as follows: the ordinate is divided into parts of intensity $1/2^n$ and the corresponding filter thicknesses are noted. Reference is then made to the standard absorption curve. The intersection of the noted filter thickness with the corresponding $n$-curve gives a sequence of energies which gives $E_0$ and $R$ as $n\rightarrow\infty$.

The method of Bleuler and Zunti is essentially that of Feather, differing only in the procedure used to obtain the range, and the absorption curve adopted as the standard. Although these workers started with Fermi allowed spectra, their standard absorption curves almost exactly fit the absorption curve of RaE.

### Widdowson and Champion Method

Widdowson and Champion[19] proposed that an aluminum absorption curve could be represented by

$$y=\sum_n a_n(R-x)^n, \tag{22}$$

[55] W. Bothe, Handbuch der Physik, 22/2, 1 (Julius Springer, Berlin, 1933).

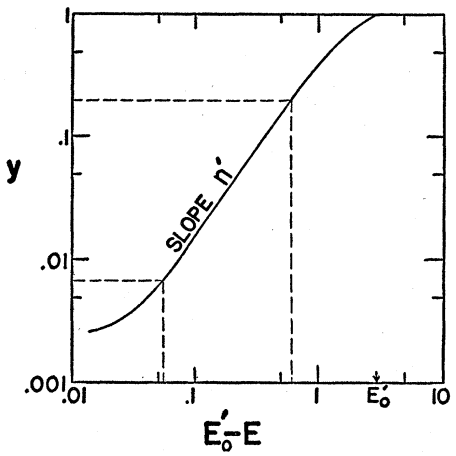


FIG. 7. Typical plot of $\log y$ *vs* $\log(E_0'-E)$ for a simple spectrum. Curving at upper end of plot shows failure of Eq. (24) to represent the experimental data at low filter thickness. Curving near the lower end of the plot results from the wrong choice of $E_0'$ in this approximation.

where $y$ is the fractional transmission, $R$ is the range thickness, and $x$ is the interposed filter thickness. In practice, they found that a single term of the polynomial was sufficient, with the value of $n$ determined by performing an experiment on a substance whose range was known. Widdowson and Champion assumed that $n$ was fairly constant for a given experimental arrangement and they found that $n=3$ or $n=4$ gave satisfactory results.

To obtain the end point, $y^{1/n}$ was plotted against $x$, and a straight line was obtained. This line crossed the abscissa axis at $R$. The end-point energy was then determined through a suitable range-energy curve.

Recently, Hughes, Eggler, and Huddleston[56] found that if it was assumed that monoenergetic electrons were absorbed in a strictly linear manner (approximately true for diffuse radiation) then it was possible to conclude from the shape of beta-spectra that the transmitted intensity should vary as the fourth power of the residual range.

Experience in our laboratory has indicated that the values of $n$ appropriate to various experimental curves vary from 1 for $Nd^{141}$ to 4.6 for $Cl^{34}$.

## Yaffe-Justus Method for Simple Spectra

During work on the nature and intensity of beta-rays backscattered from matter, Yaffe and Justus[57] discovered that the amount of backscattering was a sensitive function of the end-point energy of the scattered beta-rays. For a given beta-ray emitter (given $E_0$) the amount of backscattering is a function of the atomic number and thickness of the backscattering material. As the thickness of the material is increased, the intensity of the backscattered radiation reaches a "saturation value.[58] The amount of backscattering, after the saturation value has been reached, is a sensitive function of the atomic number of the backscatterer and the end-point energy of the beta-rays.

If a material of given atomic number and sufficient thickness is chosen as the scattering material, then the end-point energy of the unknown simple spectra may be quickly determined.

In a private communication, Dr. L. Yaffe has indicated that he believes this method to be very sensitive in the energy region below 0.6 Mev. The sensitivity decreases as energies of 1 Mev are approached because of the flattening of the backscattering curve.

In the region from about 0.1 to 0.3 Mev, the accuracy is believed to be about 3 percent. The accuracy drops to about 5–7 percent at about 0.6 Mev and is only about 25 percent at 1 Mev. As the energy increases further, the accuracy improves somewhat, reaching about 10 percent.

## The *n*th Power Method

The authors recently proposed a method for determining the range[9] which in some respects resembles that of Widdowson and Champion. They assumed that the lower part of an absorption curve can be represented by a single term in the expansion of Eq. (22), namely:

$$y=K_1'(R-x)^n. \tag{23}$$

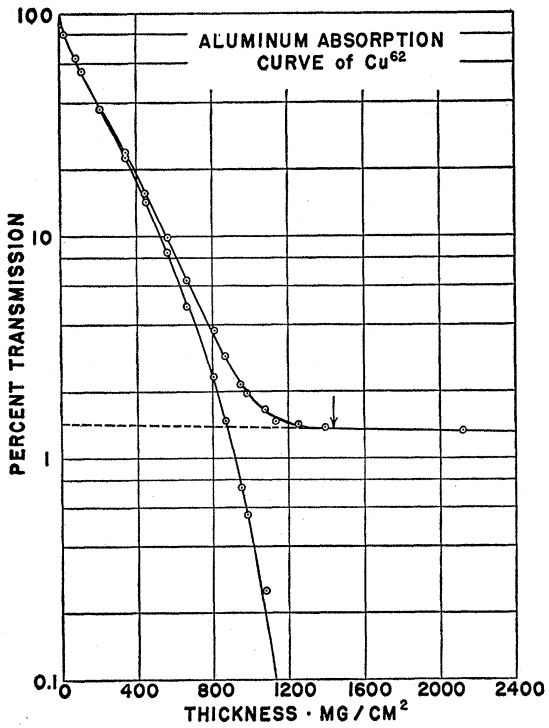


FIG. 8. Absorption curve of the $Cu^{62}$, 10.1-minute $\beta^+$-activity.

[56] Hughes, Eggler, and Huddleston, Phys. Rev. **75**, 515 (1949).
[57] L. Yaffe and K. M. Justus, Phys. Rev. **73**, 1400 (1948).
[58] L. Yaffe and K. M. Justus, J. Chem. Soc. Suppl., No. 2, 5 S341 (1949); also "Conference on Absolute $\beta$-Counting," Nat. Res. Council Preliminary Rep. No. 8 (October, 1950), p. 27.

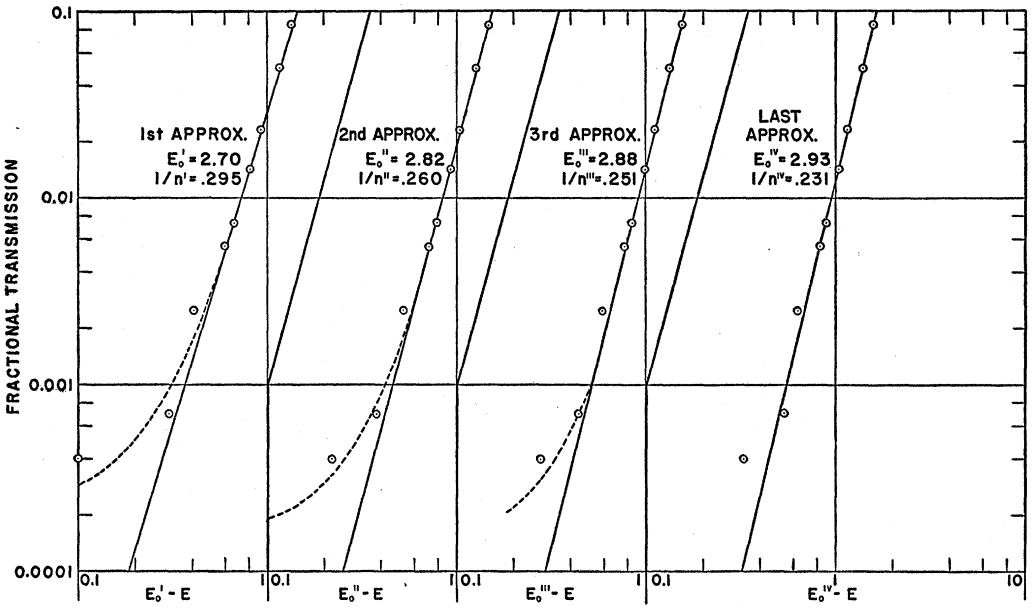


FIG. 9. The series of approximations used to obtain the correct value of $n$ for the $Cu^{62}$ absorption curve. The initial value of the end-point energy $E_0'=2.70$ was obtained from Fig. 8 by inspection, this value was used in the first approximation to obtain $1/n'=0.295$. This value of $n$ is used in the first approximation of Fig. 10 to obtain $E_0''$. $n''$ is now obtained above in the second approximation. The procedure is repeated three times. The value of $E_0=2.93$ obtained from the $\Delta E$ plot of Fig. 10 is then used in the last approximation to give $1/n=0.231$.

In this equation $y$ is the fractional transmission, $K_1'$ is a constant, $R$ is the range thickness, and $n$ is a positive constant greater than unity, but not necessarily an integer. The authors felt that if this equation is valid, then these two constants should be contained implicitly in the experimental data of $y$ as a function of $x$. It was found that better results were obtained by replacing $R$ and $x$ in (23) by the equivalent energy from a range-energy curve and writing

$$y=K_1(E_0-E)^n, \tag{24}$$

Equations (23) and (24) are not identical, because $x$ and $E$ are not linearly related. Transposing, the equation may be written

$$y^{1/n}=K_2(E_0-E). \tag{25}$$

The method adopted for solving for the constants $n$ and $E_0$ may be summarized as follows: a value of $E_0$, say $E_0'$ is obtained from the absorption curve by inspection. A plot on log-log paper is made of $y$ *vs* $(E_0'-E)$ and the slope of the curve is determined, giving a value of $n$, say $n'$. Using this value of $n'$ a plot on linear paper is made of $y^{1/n}$ *vs* $E$. From (25) it can be seen that when the ordinate is zero the value of $E$ is $E_0$. However, since experimental points are not available right up to the end point, one obtains a value $E_0''$ for the end-point energy. Using this value $E_0''$, a new value is obtained, $n''$. Using this new value of $n''$ and $E_0''$ a more accurate value for the end-point energy, $E_0'''$, can be obtained. This method of successive approximation is repeated until a sufficiently accurate value is obtained.

All the absorption curves examined by this method have yielded a sequence of values $E_0^j$ ($j=', '', ''', {}^{iv}\ldots$) which formed a convergent series. It is assumed that the limiting value of the sequence is the required end-point energy.

A typical plot of log $y$ *vs* $\log(E_0'-E)$ is shown in Fig. 7. This sketch shows the appearance of the curve when the spectrum is simple and when $E_0^j>E_0$. The curving over at high values of $y$ occurs because Eq. (24) can represent the absorption curve only in the region below its inflection point (see Fig. 1(a)). The curving at low values of $y$ occurs because $E_0^j>E_0$. $n$ should be determined in the region between the dotted lines. The determination of $n$ for complex spectra will be discussed later.

To illustrate the method we will apply it to $Cu^{62}$. The absorption curve of this spectrum is shown in Fig. 8. By inspection an end point of 2.7 Mev is obtained (1320 mg/cm$^2$), where the range energy curve of Fig. 2 has been used. The series of approximations outlined above are illustrated in Figs. 9 and 10. The value of $\Delta E=E_0''-E'$, $E_0'''-E''$, and $E_0^{iv}-E'''$ (up to third approximation) are plotted in the insert of Fig. 10, and give, by extrapolation to $\Delta E=0$, a value of $E_0=2.93$ Mev. This value is used in making a fourth approximation and it gives back the same value. Using a magnetic spectrometer, Hayward[59] has obtained $2.92\pm0.01$ Mev.

It should be noted that only the lower portions of the curves, on an enlarged scale, are plotted in Fig. 10. The complete plot of the fourth approximation is given

[59] R. W. Hayward, Phys. Rev. 78, 87(A) (1950).

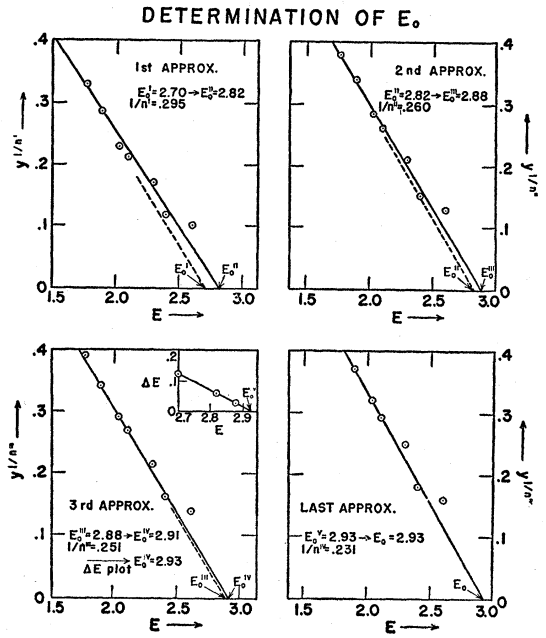


FIG. 10. The series of approximations used to obtain the end-point energy of the $Cu^{62}$ beta-spectrum. The value of $n'$, $n''$, and $n'''$ obtained from Fig. 9 are used to obtain values of $E_0'=2.82$, $E_0''=2.88$, and $E_0'''=2.91$ Mev. The plot in the insert for $\Delta E=E_0''-E_0'$, $E_0'''-E_0''$, and $E_0^{iv}-E_0'''$ against $E_0$ gives a limiting values of $E_0^v=2.93$ Mev. The fourth plot shows that $1/n^{iv}=0.231$ obtained from $E_0^v$ gives back the same value.

in Fig. 11. The experimental data as well as the computations on the first and last approximations are given in Table V.

Because the wrong value of $E_0$ is used in each of the first three approximations of Fig. 9, the lower experimental points deviate from a straight line. If accurate data are available and conversion and Compton electrons are negligible, then the value of $E_0$ required to give a straight line may be used as a criterion for obtaining the correct end-point energy.

### *n*th Power Method and Complex Spectra

The $n$th power method gives good results when applied to simple spectra. In the case of complex spectra certain difficulties arise which will now be considered. The general $y^{1/n}$ plot has the shape indicated in Fig. 12(a). Curving of the plot at low energies results from the fact that the actual beta-spectrum has a few electrons at low energies (i.e., $dy/dE\approx 0$ for $E=0$) whereas Eq. (24) implies a large initial beta-intensity contrary to the Fermi theory. The point where the deviation of the graph from a straight line becomes appreciable depends on the particular beta-spectrum being examined.

Figure 12(b) shows a typical $y^{1/n}$ plot for a complex spectrum with two components. The series of approximations necessary to obtained the high energy component $E_{01}$ are made as if the spectrum were simple, but in evaluating $n$ care must be taken to obtain the value of $n$ for the high energy component alone. The break in the curve indicates the presence of a lower energy component (compare to a Kurie plot for complex spectra[2,3]). To obtain the end-point energy $E_{02}$ of the lower component the straight line portion is extended to low energies. The value of $y$ for $E=0$ so obtained is denoted by $y_{01}$.

Once the straight line for the high energy component has been drawn, the values of $y^{1/n}$ on it, raised to the $n$th power, and subtracted from the experimental $y$'s at corresponding energies to give the $y$'s for the low energy component. The value of $E_{02}$ is then determined by the usual procedure for simple spectra.

Actually, the straight line portion of Fig. 12(b) representing the high energy component should not be extended back to zero energy as a straight line, but as a line which becomes horizontal (or nearly horizontal) at zero energy, the same as for a simple spectrum.

Because of this curving over, which has not been allowed for, the resultant values of $y_2$ for $E_{02}$ will give a peaked $y_2^{1/n}$ plot as shown in 12(b). Hence, if the end-point energy of the low energy component falls into the curving region of the high energy component then a determination of $E_{02}$ will be extremely difficult or impossible.

It has been observed that if the intensity of the low energy component is low enough, its presence may be completely masked in the curving region. The true value of $y_{01}$ depends on the branching ratio. Branching ratios cannot accurately be determined by the $n$th power method of absorption curve analysis. A fair value of the branching ratio can sometimes be obtained if $y_{01}$ is adjusted so that the curve for $E_{02}$ becomes horizontal at $E=0$.

One very important consideration in using the $n$th power method is that of having a good determination of the absorption curve background, though this is probably equally true for the other methods.

Two examples of the application of this method to complex spectra will now be presented. Yaffe[58] has published a good absorption curve for the betas from

TABLE V. Analysis of the absorption curve of $Cu^{62}$. Only the values used in the first and last set of approximations are shown in detail.

| Filter mg/cm² | Energy Mev | Fractional trans. $y$ | $E_0'=2.70$ $(E_0'-E)$ | $y^{.295}$ | $E_0^{iv}=2.93$ $(E_0^{iv}-E)$ | $y^{.231}$ |
|---|---|---|---|---|---|---|
| 31 | 0.160 | 0.794 | 2.54 | ··· | 2.77 | 0.948 |
| 81 | 0.305 | 0.617 | 2.40 | ··· | 2.63 | 0.893 |
| 120 | 0.395 | 0.544 | 2.30 | ··· | 2.53 | 0.870 |
| 220 | 0.615 | 0.367 | 2.09 | ··· | 2.32 | 0.791 |
| 353 | 0.880 | 0.2235 | 1.82 | ··· | 2.05 | 0.715 |
| 457 | 1.07 | 0.1411 | 1.63 | 0.57 | 1.86 | 0.639 |
| 571 | 1.30 | 0.0842 | 1.40 | 0.489 | 1.63 | 0.569 |
| 674 | 1.50 | 0.0490 | 1.20 | 0.406 | 1.43 | 0.494 |
| 807 | 1.75 | 0.0233 | 0.95 | 0.330 | 1.18 | 0.418 |
| 867 | 1.85 | 0.0417 | 0.85 | 0.287 | 1.08 | 0.371 |
| 945 | 2.00 | 0.0073 | 0.70 | 0.229 | 0.93 | 0.320 |
| 984 | 2.06 | 0.0055 | 0.64 | 0.211 | 0.87 | 0.293 |
| 1085 | 2.25 | 0.0025 | 0.45 | 0.170 | 0.68 | 0.248 |
| 1139 | 2.35 | 0.0007 | 0.35 | 0.118 | 0.58 | 0.181 |
| 1257 | 2.57 | 0.0004 | 0.13 | 0.101 | 0.36 | 0.160 |

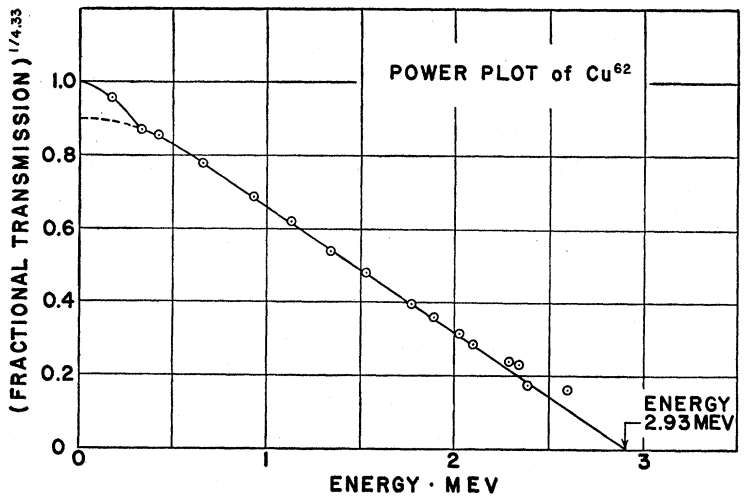


FIG. 11. Complete plot of the fourth approximation used to obtain the end-point energy of the $Cu^{62}$ positron spectrum.

$Rh^{106}$. An analysis of this spectrum gave the $y^{1/n}$ plot shown in Fig. 13. The end-point energies obtained using Eq. (8) for the range-energy relation are in good agreement with those found by magnetic spectrometer measurements.[60] D. E. Alburger has recently‡ redetermined $Rh^{106}$ and reports beta-ray end-point energies of 3.53±0.01 Mev (68 percent), 3.1±0.1 Mev (11 percent), 2.44±0.07 Mev (12 percent), and 2.0±0.1 Mev (3 percent). Figure 13 shows that although there were not sufficient points on the absorption curve used to resolve all four components, the method has sought out the highest value due to its larging weighting, and has yielded a mean of the lowest values.

Another example is that of $N^{12}$. This activity was found by Alvarez[23] and reported by him to have an end-point energy of 16.6 Mev. This value was obtained by inspection of the absorption curve and using the range-energy data of Glendenin and Coryell.[29] The published absorption curve has been analyzed by the $n$th power method (Fig. 14) and was found to give an end point of 16.6 Mev. The shape of the curve would seem to suggest the presence of a lower energy component, but this could not be resolved well since the experimental points are too sparse. It can be roughtly estimated to be at 9 Mev with an intensity 25 percent of the 16.6-Mev component.

The last two points in the $N^{12}$ curve are seen to deviate from the straight line. This effect is characteristic of a small error in determining the background and serves to illustrate the need for good background determinations.

### The $f-n$th Power Method

In the previous section we have discussed some of the difficulties which are encountered when one attempts to apply the $n$th power method to complex spectra. These limitations of the $n$th power analysis often prevent one from resolving the components of a complex spectrum and from obtaining the correct branching ratios. An attempt has been made to modify our analysis to overcome these difficulties.

The constants of Eq. (24) are chosen so that it will represent the absorption curve near its end point. A plot of this equation will cut the $y$ axis at $K_1E_0^n$, whereas the actual values of $y$, as determined experimentally, will only rise to $y=1$ at $E=0$ (see Fig. 12(a)). To make the experimental points fall on a straight line over the whole range $E=0$ to $E=E_0$ it would be necessary to write

$$y/f_1=K_1E_0^n(1-x)^n, \tag{26}$$

where $x=E/E_0$ and $f$ is some function of $E$ chosen to raise the solid curve of Fig. 12(a) to the dotted line. Since the high energy portions of the curves coincide, we must have $f_1\approx 1$ for $E$ near $E_0$, and to raise the low energy part of the solid curve $f_1$ must be less than one for $E$ less than about $E_0/2$.

Our choice of $f_1$ should be governed to some extent by the shape of the beta-spectrum. The derivative

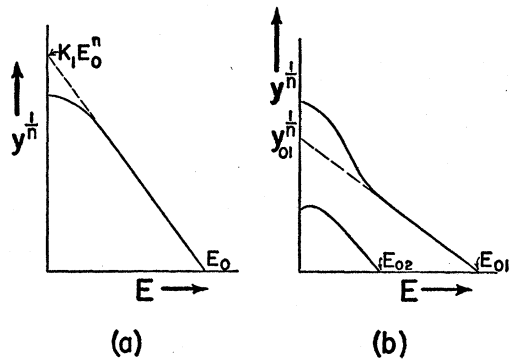


FIG. 12. (a) Plot of $y^{1/n}$ *vs* $E$ for a simple spectrum. Curving of the plot at low energies results from the fact that Eq. (24) does not represent the actual spectrum at low energies. It applies only near the end point. (b) Typical $y^{1/n}$ *vs* $E$ plot for a complex spectrum with two components. The break in the curve indicates the presence of a lower energy component. The curving over of the lower plot results from extending the high energy component to $y_{01}^{1/n}$ as a straight line rather than as in (a).

[60] W. C. Peacock, Phys. Rev. **72**, 1049 (1947).
‡ Bull. Am. Phys. Soc., Chicago meeting, October 1951, Q 12.

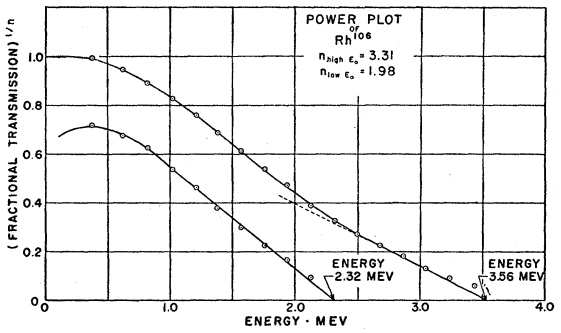


FIG. 13. Analysis of the complex $Rh^{106}$ spectrum by the $n$th power method. The absorption curve for this activity will be found in reference 58.

$dy/dE$ is the shape of the original spectrum as modified by various thicknesses of absorber and must still represent a distribution of betas which has zero intensity at the high and low energy ends. (Zero intensity at $E=0$ is not in strict agreement with the Fermi theory.) Thus $f_1$ must be chosen to make $dy/dE=0$ at $E=0$ and $E=E_0$. There are many functions which will satisfy these conditions; in particular if we desire to make $f_1$ have the form $1-ae^{-bx}$, then the foregoing conditions are satisfied by

$$f_1=1-(k/k+1)e^{-nx/k}. \tag{27}$$

At $x=0$, $y=1$ and we have $k+1=K_1E_0{}^n$. It would be desirable to renormalize our curve to meet the ordinate at $y=1$ for $x=0$. This must be done by dividing both sides by $(k+1)$, giving

$$y=f(1-x)^n=(k+1)(1-x)^n[1-(k/k+1)e^{-nx/k}]. \tag{28}$$

It is now clear that $k$ is the distance between $y=1$ and where the straight line (before renormalization) cuts the ordinate for $x=0$.

The derivative, $dy/dE$ is plotted in Fig. 15 for various values of $n$ and $k$. The curves show that the shapes of the modified spectra are only weakly dependent on $k$.

To analyze a simple absorption curve, as a first approximation it is assumed that $f=1$ $(k=0)$ and $n'$ is found from a log-log plot, similar to that of Fig. 7. A plot of $y^{1/n}$ *vs* $E$ is then made and extrapolated to $E=0$. This gives an approximate value of $k$. With this value of $k$ it is possible to compute $f$. Then a plot of $(y/f)^{1/n}$ *vs* $E$ is made yielding an end-point energy $E_0'$. A plot of $\log(y/f)$ *vs* $\log(1-x)$ will give a new value for $n$, $n''$, etc. This process may be repeated any number of times to give an accurate value of $E_0$.

Complex curves are not analyzed so easily. In this case it is not possible to solve for the value of $k$ directly. We have found that as a first approximation it is possible to take $k=1$ and to perform an analysis. If the low energy components resulting from this analysis have $dy/dE$ other than zero at $E=0$, $k$ must be adjusted until this is the case.

From the foregoing descriptions of the $f-n$th power method it is evident that it has by no means been fully developed nor is it easy to apply. Each absorption curve analyzed requires individual and careful handling. The method bears similarity to the treatment of magnetic spectrometer measurements of forbidden beta-spectra by the use of a Kurie plot. The function $f$ may be compared to the product of the Coulomb factor and the "forbidden" correction term used in such a plot.

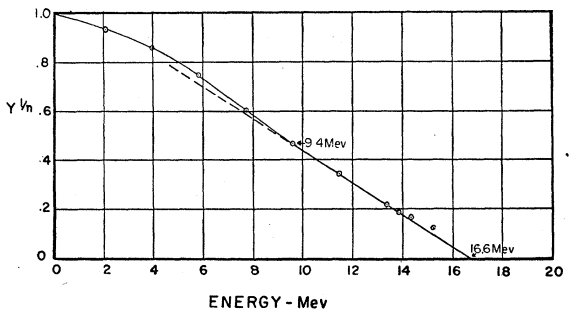


FIG. 14. Analysis of the absorption curve for the betas from $N^{12}$ as published by Alvarez.[23] This graph indicates a second component of about 9-Mev end point and about $\frac{1}{4}$ of the intensity of the 16.6-Mev component.

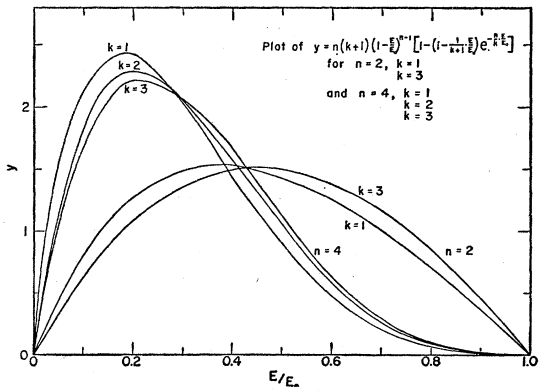


FIG. 15. Dependence of the $(dy/dE)$ from Eq. (28) upon $k$ and $n$.

With careful handling of this method complex spectra may be analyzed even though the lower component is in the curving region. Quite good branching ratios can also be obtained. As an example of its use the reader is referred to reference 10 wherein the absorption curve of $Cl^{39}$ was analyzed. This analysis is reproduced here in Fig. 16. Two components and possibly a third at quite low energies were found. Coincidence work supported the existence of two of these. The third occurred at such low energies that it was well into the curving region of the high energy component and so its presence is doubtful.

The values of the energies and ranges of $Mn^{56}$ given in Table IV were determined by the $f-n$th power method and good agreement with spectrometer measurements is found. The branching ratios determined are also in good agreement.

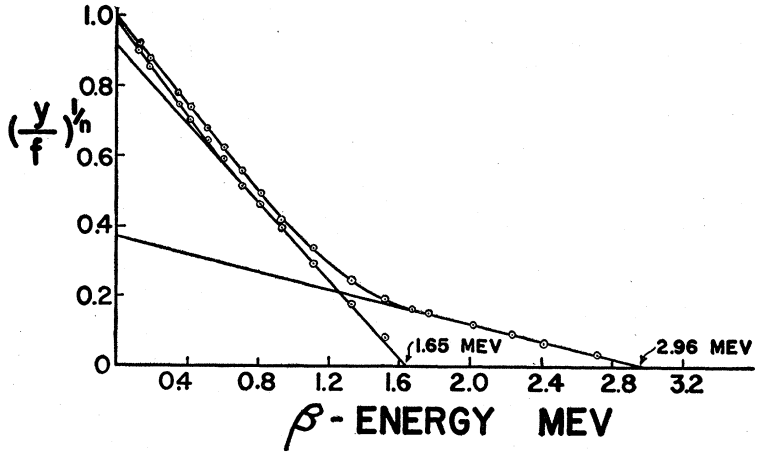


FIG. 16. Analysis of the absorption curve of $Cl^{39}$ betas by the $f-n$th power method. The two higher energy components were substantiated by coincidence measurements in reference (10).

### Conversion Electrons

Conversion peaks will show up on the $y^{1/n}$ plot or the $(y/f)^{1/n}$ plot as sharp discontinuities in the curves. Their magnitude can thus be ascertained and then the peak can be subtracted from the data. Such a peak was observed in the $Cl^{39}$ analysis and was confirmed by coincidence measurements.

Some substances have a great many conversion peaks, and the area under these peaks may be greater than that under the beta-spectrum itself. In this case the methods outlined here are completely useless. One such a substance[61] is $Hf^{181}$.

## DISCUSSION

The determination of beta-end-point energies rests upon a number of assumptions which are more often implied in the method used rather than stated explicitly. These assumptions will now be examined and their bearing on the validity of the various methods discussed.

An analysis of the manner in which electrons are absorbed in a solid should lead to a better understanding of the whole problem and point out the factors to be taken into consideration in order to avoid errors.

The usual arrangement of apparatus for obtaining an absorption curve consists of a radioactive source, a detector some distance from it, and intervening absorbers whose thickness may be varied. Let us assume for simplicity that the electrons from the source are monoenergetic and that no gamma-rays are present. Initially with no absorber between itself and the source, the detector will have a response proportional to the solid angle which it subtends at the source. The introduction of thin sheets of absorber will cause some of the electrons in the beam, originally directed towards the counter, to be scattered with a resulting decrease in the response of the detector. As the thickness of the absorber is increased, the number of electrons suffering single and multiple collisions increases with corresponding divergence in the beam originally contained within the detector solid angle and a further decrease in detector response. Eventually, for very thick absorbers, the divergence of the beam will become so large that the electrons will completely lose their original direction of motion and take random directions within the absorber. Further increase in absorber thickness will only change the density of electrons and not their distribution. The process will now resemble the case of diffusion. Bothe[55] has described in detail the foregoing process of electron absorption.[62] Using the equations of Bothe, Fowler *et al.*[37] have been able to show that for high energy particles the depth of penetration $x_d$ within an absorber, where multiple scattering may be considered to end and diffusion to set in, is given by the following equation:

$$x_d=(E_0+1/E_0+7.5)R_0, \tag{29}$$

where $R_0$ is the range of particles whose energy was initially $E_0$. In this equation it is assumed that the effective solid angle of the setup is of the order of one steradian.

For absorbers whose thickness is less than $x_d$, multiple scattering is the main cause of absorption and thus the actual amount of radiation reaching the detector is strongly dependent on geometry. On the other hand, for an absorber thickness greater than $x_d$, the diffusion process is predominant with a resulting decrease in sensitivity to geometry. Sensitivity to geometry implies not only the relative position of source and detector but also the position of the absorbers between them. A good example of the effect of absorber position on the shape

[61] K. Y. Chu and M. L. Wiedenbeck, Phys. Rev. **75**, 226 (1949).

[62] Bethe, Rose, and Smith (Proc. Am. Phil. Soc. **78**, 573 (1938)) have described electron absorption as follows: "A beam of fast electrons will in the beginning of its path suffer energy loss but very little scattering and thus move in almost a straight line. With decreasing energy, scattering will become more important until finally the stage of diffusion is reached where the direction of motion becomes almost random." From this point of view the initial process of electron absorption is quite different from that assumed by Bothe. There is little experimental evidence to decide whether absorption or scattering is the major cause of electron removal in thin absorbers.

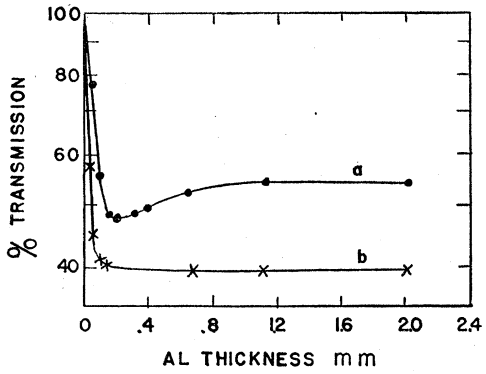


FIG. 17. Effect of absorber position and resulting Compton electrons on the shape of an absorption curve according to Meitner.[63] (a) Absorbing foils near the source. (b) Absorbing foils near the detector.

of the absorption curve will be found in reference 37, Figs. 7–9.

So far we have discussed the absorption of the beam of homogeneous electrons. The same analysis will apply to nuclear beta-spectra. In this case the absorption curve shape will be an even stronger function of geometry since the value of $x_d$ depends on the initial energy of the electrons, which now has values between 0 and $E_0$. Other factors which will effect the absorption curve shape have been enumerated in the discussion of the Feather method. The reason geometry does not play an important part in the Feather method when applied to simple spectra now becomes evident; comparison with the standard curve is made only at large absorber thicknesses. The relative insensitivity of the shape of the absorption curve near the end-point to geometry also helps to explain why range energy measurements in various laboratories are in fairly good agreement with each other. It has already been shown that detector sensitivity has little effect on the measured range.

A discussion of the absorption method for determining end-point energies is not complete without a word of caution. The method has only limited usefulness and may lead to erroneous conclusions unless great care is exercised in obtaining the absorption curve as well as in interpreting it. In some cases, the nature of the spectrum is such as to make it almost impossible to determine the end point.

The effect of soft gamma-rays on the absorption curve has been discussed by Meitner.[63] She proposed a method for determining the energy of gamma-rays accompanying beta-decay from the change in shape of the absorption curve taken under different experimental conditions. It is based on the effect which Compton electrons (resulting from the gamma-rays) have upon the shape of the curve. Meitner's analysis may be used to point out some of the difficulties encountered in aluminum absorption work.

Following Meitner, we consider the usual experimental arrangement of a radioactive source some distance from a detector and an intermediate absorber. If the absorber is larger in area than the source, which is usually the case, and if the absorber is very close to the source, then because of the special directional distribution of Compton electrons, many of the Compton electrons reaching the detector will come from gamma-rays not originally included in the detector solid angle. This experimental arrangement will give undue emphasis to the Compton electrons. The effect will be particularly pronounced at large absorber thicknesses where the intensity of beta-rays reaching the counter is low and the intensity of the Compton electrons is large.

When the end-point energy of the beta spectrum is lower than that of Compton electrons, the absorption curve will be very distorted and may even go through a minimum value, beyond which the counting rate increases with increasing absorber thickness. A striking example of this effect is illustrated by curves (a) and (b) of Fig. 1 of Meitner's article and reproduced here in Fig. 17. To obtain these curves a Scandium 46 source, supported on an aluminum sheet 0.1 mm thick, was mounted 5.5 cm from the detector. Curve (a) was taken with the absorbing foils near the source and curve (b) with the absorbing foils next to the detector.

When the foils are near the detector, only those gamma-rays which were originally directed into the detector can give rise to Comptons which are counted. This reduces the effect of the Compton electrons with a corresponding decrease in the distortion of the absorption curve. Thus it should be emphasized that in order to minimize the effects of Compton electrons the absorbers should be placed as close as possible to the detector.

The authors would like to thank Dr. C. E. Mandeville of the Bartol Foundation and Dr. L. Yaffe of Chalk River for making available to them some beta-ray absorption curves. They would also like to thank Dr. B. W. Sargent for proofreading the first part of this paper and for making many valuable suggestions. One of the authors (A.P.) is indebted to the Canadian National Research Council for a bursary which enabled him to continue with this work.

[63] Lise Meitner, Phys. Rev. **63**, 73 (1943).